VHMPID RICH prototype using pressurized C_4F_8O radiator gas and VUV photon detector

T.V. Acconcia [a], A.G. Agócs [b], F. Barile [c], G.G. Barnaföldi [b], R. Bellwied [d], G. Bencédi [b], G. Bencze [b,*], D. Berényi [b], L. Boldizsár [b], S. Chattopadhyay [e], D.D. Chinellato [d], F. Cindolo [f], K. Cossyleon [h], D. Das [e], K. Das [e], L. Das-Bose [e], A.K. Dash [a], S. D'Ambrosio [f], G. De Cataldo [c], S. De Pasquale [f], D. Di Bari [c], A. Di Mauro [g], E. Futó [b], E. Garcia-Solis [h], G. Hamar [b], A. Harton [h], G. Iannone [f], R.T. Jimenez [i], D.W. Kim [j], J.S. Kim [j], A. Knospe [k], L. Kovács [b], P. Lévai [b], C. Markert [k], P. Martinengo [g], L. Molnár [b,g], E. Nappi [c], L. Oláh [l], G. Paić [i], C. Pastore [c], G. Patimo [f], M.E. Patino [i], V. Peskov [i,g], L. Pinsky [d], F. Piuz [g], S. Pochybová [b], I. Sgura [c], T. Sinha [e], J. Song [m], J. Takahashi [a], A. Timmins [d], J.B. Van Beelen [g], D. Varga [l], G. Volpe [c], M. Weber [d], L. Xaplanteris [k], J. Yi [m], I.-K. Yoo [m]

[a] UNICAMP, University of Campinas, Campinas, Brazil
[b] Wigner RCP of the HAS, Budapest, Hungary
[c] INFN Sezione di Bari & Universitá degli Studi di Bari, Dipartimento Interateneo di Fisica M. Merlin, Bari, Italy
[d] University of Houston, Houston, USA
[e] Saha Institute, Kolkata, India
[f] University of Salerno, Salerno, Italy
[g] CERN, CH1211 Geneva 23, Switzerland
[h] Chicago State University, Chicago, IL, USA
[i] Instituto de Ciencias Nucleares Universidad Nacional Autonoma de Mexico, Mexico City, Mexico
[j] Gangneung-Wonju National University, Department of Physics, Gangneung, South Korea
[k] University of Texas at Austin, Austin, USA
[l] Eotvos University, Budapest, Hungary
[m] Pusan National University, Department of Physics, Pusan, South Korea

ARTICLE INFO

ABSTRACT

A small-size prototype of a new Ring Imaging Cherenkov (RICH) detector using for the first time pressurized C4F8O radiator gas and a photon detector consisting of MWPC equipped with a CsI photocathode has been built and tested at the PS accelerator at CERN. It contained all the functional elements of the detector proposed as Very High Momentum Particle Identification (VHMPID) upgrade for the ALICE experiment at LHC to provide charged hadron track-by-track identification in the momentum range starting from 5 potentially up to 25 GeV/c. In the paper the equipment and its elements are described and some characteristic test results are shown.

1. Introduction

The idea of the Very High Momentum Particle Identification Detector (VHMPID) [1,2] upgrade project and the focusing Ring Imaging Cherenkov (RICH) detector as a technical solution of the concept are described in several papers and documents [3–5]. The VHMPID detector has been proposed to enhance the track-by-track particle identification (PID) capabilities of the ALICE experiment at LHC [6] for charged hadrons (p, π, K) in the momentum range from 5 potentially up to 25 GeV/c and with this to extend its range to higher momenta with respect to the present 2–5 GeV/c provided by the already running HMPID (High Momentum Particle Identification Detector) [7].

According to the conceptual design the full VHMPID is composed of several large lateral-size modules of about 2.5 m in the beam direction of the ALICE experiment and 1.5 m perpendicular
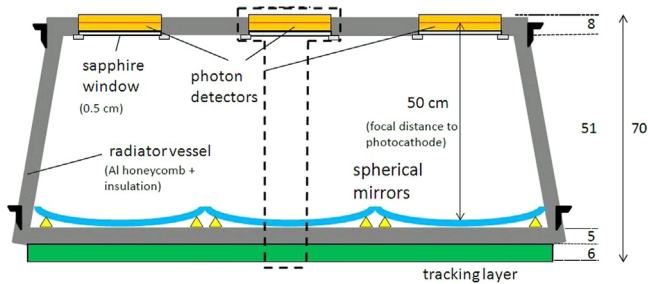
Fig. 1. Schematic view of the VHMPID module in $\eta=0$ region. Dashed line: the test prototype compared to the full module.

Fig. 2. A typical spectral quantum efficiency curve (after [9]).

to it (see [1]). The longitudinal dimension of the modules is determined by the available space in ALICE in front of the electromagnetic calorimeter (DCAL) leaving about 70 cm length for the full unit. This gives an upper limit of about 50 cm for the length of the radiator with the photon detector. The schematic view of the module planned for the $\eta=0$ region is shown in Fig. 1.

Profiting from the experience of the ALICE HMPID detector [7]) the baseline option for the single-photon detection is a multiwire proportional chamber (MWPC) equipped with CsI photocathode, sensitive in the VUV spectral range below 200 nm and operated in pure methane (CH_4) [8].

The choice of the radiator is determined by the particle type to be identified and the momentum range of interest. Our needs require a radiator with refractive index of about 1.005–1.006. The proposed technical solution is a gaseous radiator volume filled with octafluorotetrahydrofuran (C_4F_8O) pressurized up to 3.5–4 bar (2.5–3 bar overpressure) and, to avoid condensation, heated up to 50 °C. The generated Cherenkov light is reflected from a spherical mirror and reaches the photon detector through a sapphire window separating the radiator volume from the photon detector. The radiator media and the geometry define the Cherenkov ring diameter at saturation which is about 10 cm. The number and size of the mirrors (consequently the number and size of the photon detector units and the number of readout channels) in one module is the result of an optimization and leads to 9–12 mirrors with 350–500 mm linear size and the same number of photon detectors of about 18×24 cm^2 active surface.

The VHMPID is completed by tracking detectors installed behind and, if the available space is enough, also in front of the Cherenkov-part to determine the location and direction of the incoming particle. If the front-detector is not installed the impact point can be reconstructed from the data of the inner ALICE detectors (TDC, TRD).

To experimentally prove the concept briefly described above and to study the functionality of its elements a VHMPID prototype has been built and tested at the T10 experimental zone in the East Hall of the PS accelerator at CERN. It contained all the elements of the proposed VHMPID detector. The lateral dimensions of the radiator allowed us to detect the full Cherenkov ring of the particle coming from the test-beam. The photon detector size corresponded to one unit of the segmented photon detection scheme.

In this paper we collect and describe the technical aspects of the experimental setup. In chapter 2 the elements of the system: the photon detector with the readout, the radiator gas part, the radiator vessel with the window, the radiator gas control system, the mirror and the tracking detectors are discussed. In chapter 3 the test setup is described, in chapter 4 some characteristic results are shown.

It has to be mentioned that a setup using pressurized heated elements, high voltage and flammable methane gas is classified as equipment of high risk. The safety-aspects had to be taken into
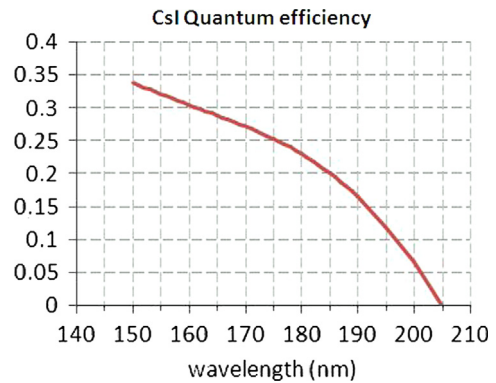
account during the design, the material choice, the construction and operation.

2. Elements of the system

2.1. Photon detector

The photon detector is an MWPC with CsI photocathode based on the HMPID experience. The R&D and construction of such chambers is described in detail in [7,8]. The most delicate part of this chamber type is the photosensitive CsI layer evaporated on the cathode plane. The R&D of the CsI-based photon detectors and the technology of the layer production are described e.g. in [9,10] where further literature can also be found. A typical spectral quantum-efficiency curve extracted from the mentioned literature is shown in Fig. 2.

As it can be seen the CsI layer is operational in the VUV spectral range starting from about 205 nm (6.2 eV). The efficiency beyond 150 nm (8.3 eV) is not relevant for our application due to the absorption of the radiator gas and possibly of the window (depending on the selected material). A non-uniformity below 10% over the full surface of the cathode can be guaranteed by the CsI production technology.

For the VHMPID prototype we used a fully renovated test-chamber of 24×13 cm^2 active area originally built for HMPID-related studies (Fig. 3 and Fig. 5). The chamber has a special feature of the possibility to change the anode–cathode gap during the test. It is equipped with pad-segmented cathode coated with a 300 nm thick CsI layer (Fig. 4). The anode plane is composed of 20 μm gold plated W/Rh wires with 4 mm pitch. The pad size is 4×8 mm^2 (8 mm perpendicular to the anode wires, 60×16 pads altogether). The anode–cathode gap is adjustable in the range of 0.8–2 mm. Two wire planes are installed in the chamber: a cathode plane made of 100 μm diameter gold plated Cu/Be wire, spaced by 2 mm and the collection electrode composed of the same wire spaced by 5 mm. This latter is collecting the electrons produced by primary ionization between the cathode wire plane and the window. The cathode layers are at ground potential, the collection electrode is set to $+400$ V. The anode plane tension is typically $+1500$ V to 2100 V depending on the gap. The chamber is mounted on the radiator and closed by the window. The chamber is operated with pure methane (CH_4). Due to the well known sensitivity of the CsI layer to air (especially humidity) the cathode was kept under gas (typically Ar) all the time: during transportation, chamber assembly, test and storage.

2.2. Front-end electronics (FEE)

The Front-End Electronics (FEE) used for the readout of the photon detector was identical to the HMPID one [11], in fact we
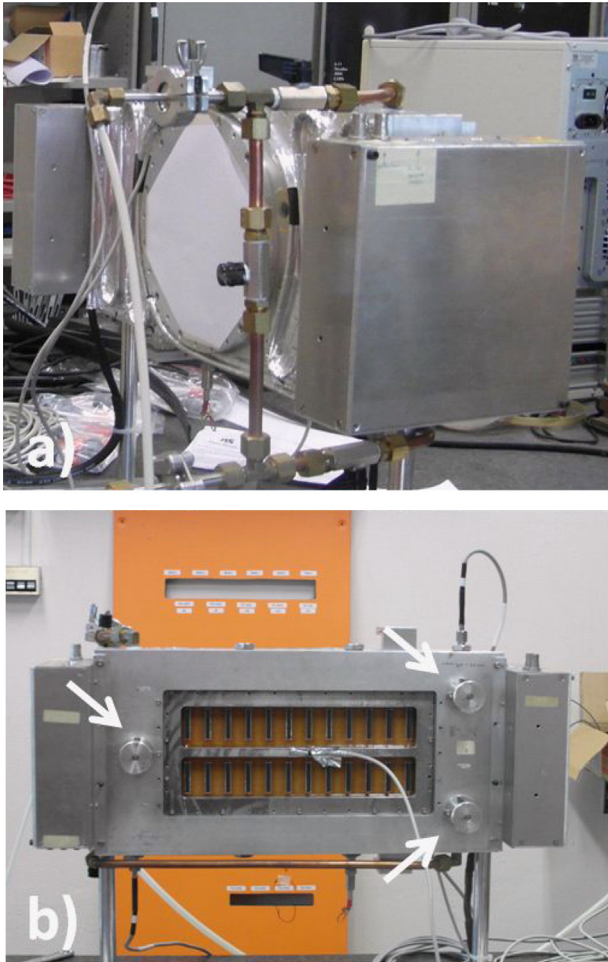
Fig. 3. The photon detector chamber. (a) The window side; (b) the front-end side (white arrows: gap adjustment).
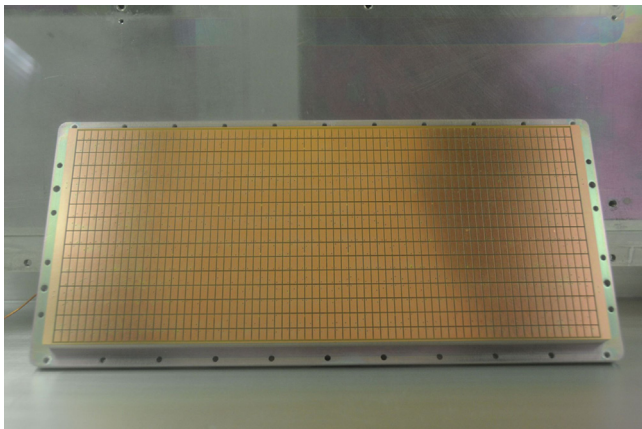

Fig. 4. The pad-plane of the photon detector with 4×8 mm^2 pads.

used some of the spare cards. The card is based on a GASSIPLEX chip in 0.7 μm technology which has a peaking time of 1.1 μs and performs multiplexed analog readout achieving 1000e noise on detector with a maximum trigger rate of 200 kHz. In Fig. 5 the photon detector chamber equipped with frontend cards is shown. The picture was taken during a preparatory test with liquid radiator to check the chamber performance at different anode–cathode gaps.
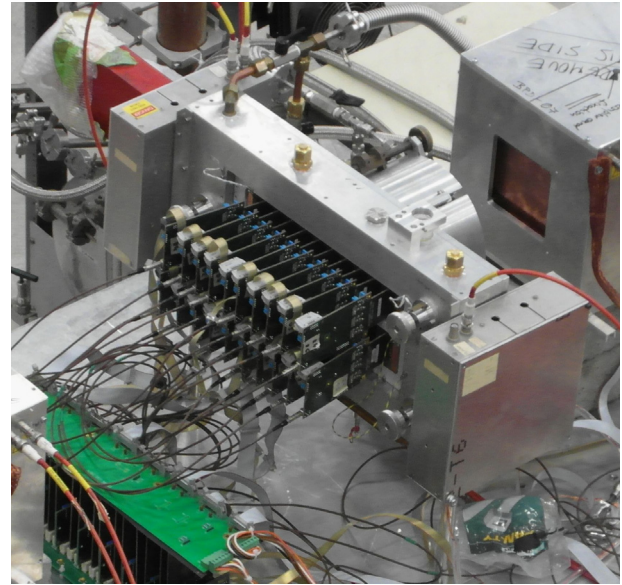

Fig. 5. The photon detector chamber with FEE cards during the preparatory test.

The HMPID frontend electronics was working satisfactorily during the test but its limited speed can prevent it from future application. Possible alternatives are discussed in [2].

2.3. Radiator gas

The required parameters of the radiator gas are determined by the momentum range of the hadrons to be detected and the chosen photon detector. In our case this is leading to the need of a radiator gas transparent in the VUV (150–200 nm) spectral range and having refractive index in the range of 1.005–1.006. The commonly (e.g. DELPHI [12], HERMES [13], HERA-B [14], HADES [15], COMPASS [16], DIRAC-II [17], LHCb [18]) used perfluorobutane (C_4F_{10}) has a refractive index of 1,0014 (at 200 nm) to 1,0017 (at 155 nm) at athmospheric pressure. By pressurizing the radiator gas up to 3.5–4 atm the refractive index and the Cherenkov emission thresholds can be tuned to the required value according to the formula $n(P) = 1 + (n_o - 1) * P$ where n_o and n are the refractive indices at atmospheric and P pressure respectively.

Also, due to the increase of the refractive index with the pressure even the relatively short (50 cm) radiator could guarantee the photon yield and ring radius at the design values for PID performance. The increase of the pressure leads to higher boiling point of the gas (see Fig. 6, the calculations were based on [19]). To avoid condensation the whole chain of the radiator gas system from the supply cylinder to the photon detector and the return line had to be heated up to 50 °C.

As the production of the C_4F_{10} gas has been discontinued at the 3 M company and it became difficult to procure it with high enough purity necessary for such application we have chosen octafluorotetrahydrofuran (C_4F_8O). This gas has already been used as radiator gas for Cherenkov-detectors [20,21] but with a photon detector working above 200 nm. There was no direct information on the behaviour and the properties of the C_4F_8O gas in VUV.

For the tests we used C_4F_8O (CAS: 773-14-8) purchased from SynQuest Laboratories, Inc. (Alachua, FL, USA) .

The C_4F_8O gas is non-toxic. Its physical and chemical properties from detector-building point of view were studied and described in [21] and were found harmless for the surrounding material (viton sealing, etc).
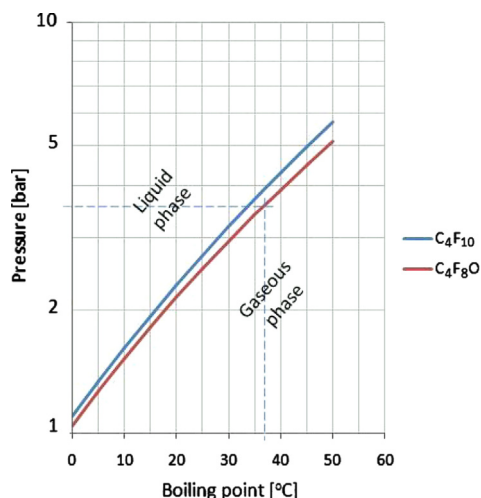
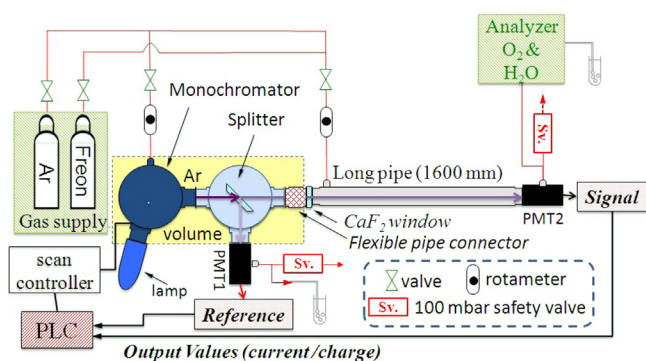Fig. 6. The calculated boiling point dependence on pressure for C_4F_{10} and C_4F_8O.

Fig. 7. The schematic view of the radiator gas transparency-meter.

2.4. Radiator gas transparency-meter and the gas quality

In order to avoid the absorption of the Cherenkov photons the cleanliness of the radiator gas is a crucial requirement. This is especially true in the VUV range where both O_2 and H_2O have a large absorption cross-section and the organic contamination usually present in the gas can reduce the transparency. To monitor the gas quality during the tests a gas transparency-meter has been built. Its structure was quite similar to the Compass solution [22] and technically also close to the device used for the HMPID [23] though this latter is used for liquid radiator (C_6H_{14}). The schematic view of the transparency meter and the setup (installed at the experimental zone) are shown in Figs. 7 and 8 respectively.

The commercial part of the device is composed of a motorized Model 234/302 holographic monochromator illuminated by a Model 632 deuterium lamp through a Model 615 reflective condenser and driven by a Model 789A-3 Digital Scan Control and Motor Driver, all from McPherson (MA, USA). The rest of the elements (besides the HAMAMATSU R6836 photomultipliers and the uncoated CaF_2 splitter and window) was made at CERN.

As the first step the device was calibrated by the following steps. Both the Ar volume and the 1600 mm long tube were filled with Ar. Then the spectrum relevant for our application (200–150 nm) was scanned and the currents in both PMTs recorded simultaneously. This calibration data was used for corrections. For the radiator gas transparency measurement the long tube was filled with the radiator gas and the spectral scan was repeated regularly during the test. The scan and the data taking were controlled by a PLC (Programmable Logic Controller) system
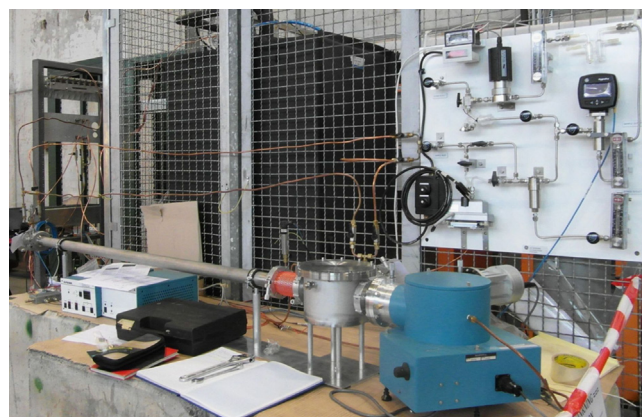

Fig. 8. The transparency-meter and the O_2 & H_2O analyzer panel (upper part on the right) at the experimental zone.
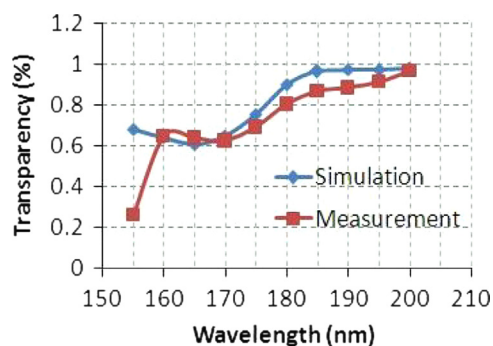

Fig. 9. The measured radiator gas transparency and its comparison with simulation (for O_2 and H_2O contaminant only).

running under PVSS control software (German abbreviation for "Process visualization and control system").

An additional gas quality control unit was built for direct measurement of the O_2 and H_2O in the radiator gas using commercial O2X1 and HygroPro sensors from GE Sensing & Inspection Technologies GmbH (see the white diagnostic panel in Fig. 8).

The transparency of the C_4F_8O gas was measured after its arrival. The result is shown in Fig. 9. The O_2 and H_2O contents were measured directly and the measured 3 ppm and 21 ppm respectively were well below the values guaranteed by the supplier. This contamination can explain most of the transparency degradation seen in the Figure. To prove this a simulation program was used (thanks to COMPASS colleagues) to calculate the transparency of a fully transparent gas with the measured O_2 and H_2O contamination and compared to the transparency measurement of C_4F_8O (also shown in Fig. 9). The difference above 180 nm was associated with organic contaminations, the fall below 160 nm is probably due to the absorption of the gas itself similar to C_4F_{10} (see e.g. [22]). The final conclusion was that the purchased gas could be used for the beam test but before its usage in real experiments a pre-cleaning would be required. The COMPASS pre-cleaning method and system described in [22] could be a good solution.

No dedicated measurements of the refractive index for C_4F_8O have been made in the 200–150 nm spectral range by us. Our expectations concerning this parameter were based on the visible similarity to the better studied C_4F_{10}. The final proof came directly from the results of the beam-test discussed in Section 4.

2.5. Radiator gas supply rack

The radiator gas supply rack and its schematic drawing are shown in Figs. 10 and 11. The rack was designed in collaboration

Fig. 10. The radiator gas supply rack. (a) The rack after assembly during the leak test; (b) the C_4F_8O cylinder and the rack (both heated and insulated) installed in the gas zone of the experimental area.
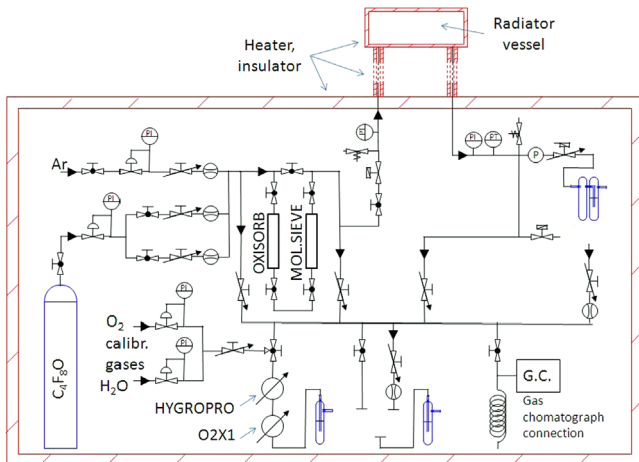

Fig. 11. The schematic drawing of the radiator gas rack and supply system.

with the CERN Detector Infrastructure (PH-DT-DI) group and built by them. It had two selectable gas inputs: one for Ar and one for the (heated) C_4F_8O. The vacuum pump was used for quick gas exchange in the radiator vessel. The full rack is heated and insulated to keep the inner temperature at the desired value up to 50 °C. Two installed filters (oxisorb and molecular sieve) could reduce the O_2 and H_2O contents of the incoming gas. In addition to the diagnostic panel mentioned in section 2.4 the rack itself was also equipped by built-in O2X1 and HygroPro sensors optionally switchable to the input gas, to the gas after the filter or to the gas returning from the radiator vessel. The data is recorded through the PLC-PVSS control system (see section 2.9). Connection points

are providing possibilities to optional diagnostic elements as the transparency meter, additional O_2 and H_2O analyzer or gas chromatograph and to calibrate these devices by etalon gas with known O_2 and H_2O contents.

2.6. Radiator vessel and the window

The radiator vessel that holds the pressurized heated C_4F_8O gas is a 590 mm long stainless steel tube of 160 mm diameter (12 liter of gas volume). It is sealed on one end by a lid supporting the spherical mirror and on the opposite end by a sapphire window which acts also as optical transmitter between the radiator and the photon detector. According to the safety rules the vessel must be designed and tested for the pressure value exceeding the nominal 3.5 bar by a factor of 1.43 for not less than 30 min [24]. Therefore the vessel was designed for the pressure range of 0–5 bar (absolute). The requirement to stand also vacuum is explained by the desire to pump the vessel in order to exchange the gas in the radiator rapidly and also clean it by pumping and heating cycles.

Two window materials were considered: sapphire as baseline and quartz as an alternative solution (cheaper, easier to manufacture). Finite element calculations during the design have shown enough rigidity and acceptably small deformation in case of 5 mm thick sapphire or 15 mm thick quartz window. During the beam test we used the 5 mm thick 165 mm diameter HEM VUV grade sapphire window [25] purchased from CM Scientific Ltd (Silsden, UK). As the sapphire has very high refractive index and considerable dispersion in the 200–150 nm spectral range it was covered by antireflective coating on both sides keeping the reflection losses below 1% in the full spectral range for 0–20 degree of angle of

incidence of the photon. The transparency of the window used in the test is shown in Fig. 12. The losses are originated in the absorption of the material itself. It should be noted that the sapphire is a birefringent crystal, however, in our application and at the given geometry this effect can be neglected.

The vessel passed a pressure test with both the sapphire and quartz windows. The pressure was kept at 5 bar for 1 h, no leak, no damage, no inelastic deformation could be observed.

2.7. Mirror

The Ø 160 mm, ROC (radius of curvature)=1000 mm spherical mirror had carbon-fiber substrate, similar to that developed for LHCb RICH [26] produced by CMA Inc. (Tucson, AZ, USA). The technology is described in detail in the quoted reference. Special effort has been made to minimize the material, weight and thickness of the substrate and, as the mirror is installed inside the radiator vessel, to minimize the long-term outgassing. The holes on the back cover help to get rid of air stuck in the reinforcing structure of the mirror substrate by pumping. The substrate was coated at CERN with Al/MgF$_2$ for maximum reflection in the VUV. The substrate before coating is shown in Fig. 13. The measured reflectivity of the coated mirror is shown in Fig. 14.

2.8. The radiator and photon detector heating

The radiator and the photon detector were fixed to each other composing a single unit. As it has been mentioned earlier the radiator gas has to be heated in the full pressurized section up to 50 °C. Heat flow studies with computational fluid dynamics (CFD) software package Fluent 6.0 were carried out to optimize the

radiator heating in the presence of the attached photon detector. The thermal dissipation of the frontend electronics was also measured by a FLUKE Ti25 thermal imager but it was found nonrelevant ($ < 4$ °C). The simulation results showed the necessity to heat not only the radiator vessel but also the detector (on the vessel side as it is seen in Fig. 15 where the calculated temperature distribution is shown for the following input parameters: the incoming pressurized (to 3.5 bar overpressure) radiator gas temperature is 40 °C, the temperature of the incoming methane and the surrounding environment is 10 °C (in view of the fact that the beam test was scheduled for November). As the figure shows this solution is safe and excludes any condensation of the radiator gas (it remains well above 36 °C).

The heating of the radiator and the chamber was made according to the simulation results as it can be seen in Fig. 16 showing the heating electric wires before putting the insulation on.

2.9. Sensors and the radiator gas control system

The radiator gas pressure and temperature regulation, the readout of the O$_2$ & H$_2$O analyzer and also the operation of the transparency meter were controlled and the data recorded by a PLC-based hardware and PVSS software. The pressure was measured in the supply and return lines at the radiator gas rack and at the inlet and outlet in the radiator vessel by pressure sensors. The temperature was measured at the gas cylinder, in the radiator gas rack, on the supply and return lines, at six points (3 top, 3 bottom) along the radiator vessel, at several points on the photon detector and the methane supply and return by temperature sensors. During the operation the starting pressure of the gaseous phase
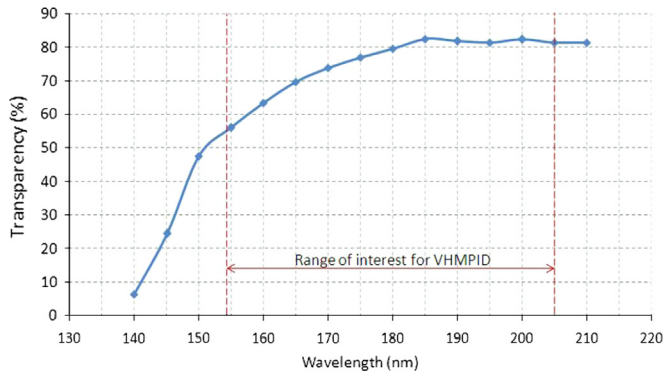
Fig. 12. The measured transparency of the antireflection-coated sapphire window (normal angle of incidence).
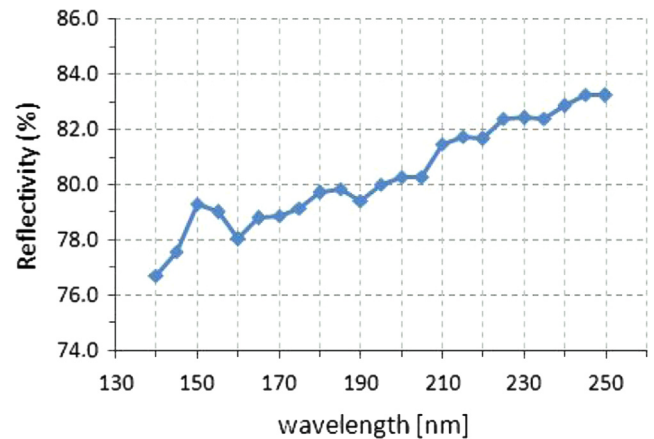
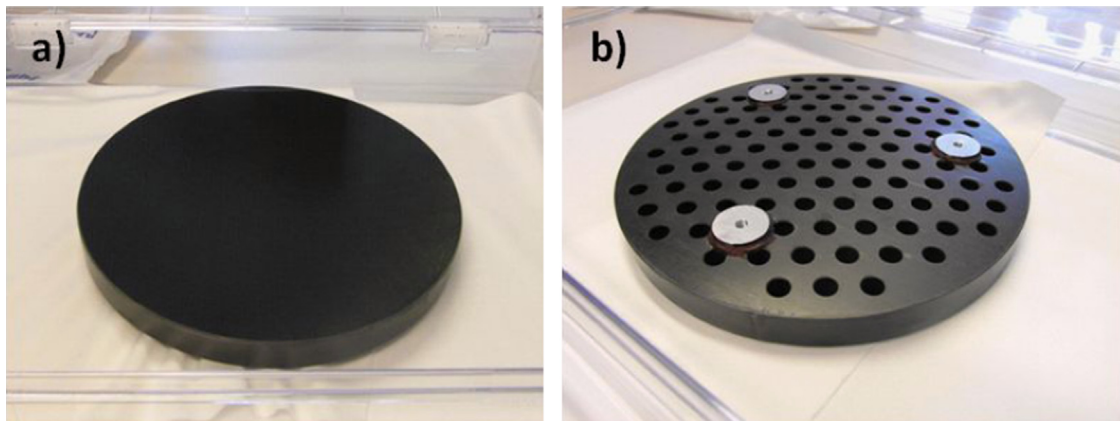**Fig. 14.** The measured reflectivity of the mirror after coating.

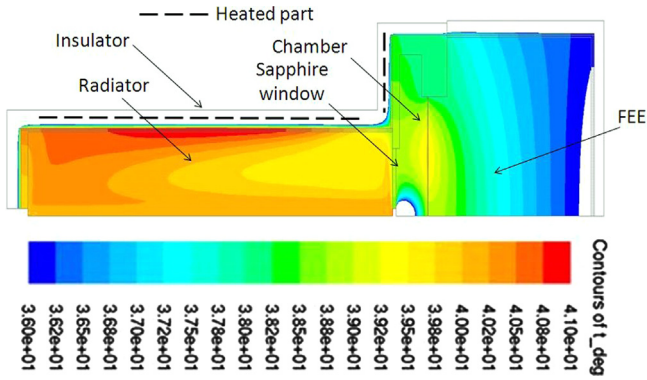**Fig. 13.** The mirror substrate front (a) and back (b) side.

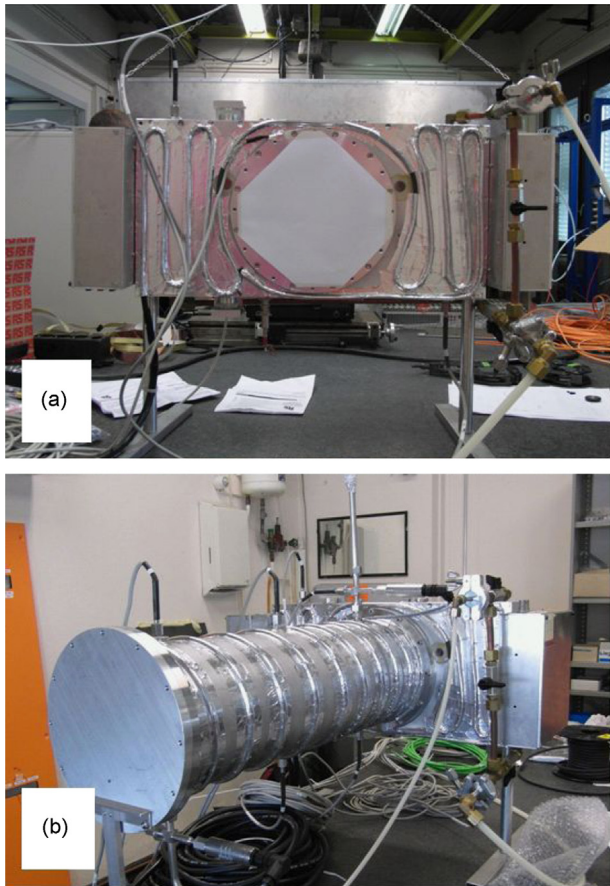Fig. 15. Simulation of the heat flow in the radiator and the photon detector.

Fig. 16. (a) The heating wires on the photon detector (b) the heating wires on the radiator and the attached photon detector.

of C_4F_8O in the cylinder was regulated by the temperature of the cylinder. The pressure inside the radiator vessel was kept by the proper operation of the electric valves at the inlet and outlet side in the radiator gas rack. The PVSS control panels for the pressurized part and the transparency meter are shown in Figs. 17 and 18 respectively. The PLC-rack is shown in Fig. 22.

2.10. Tracking (BPD) detectors

The tracking detectors (called also BPD = Beam Position Detector) one in front and the other behind the Cherenkov-part play an important role in the VHMPID-concept. The front chamber is defining the impact point of the particle. The rear chamber together with the front one- defines the trajectory inside the Cherenkov unit and helps in the matching of the trajectory with the inner ALICE tracking detector data. The information about the trajectory inside the VHMPID detector can be used to improve the ring finding algorithm and the resolution of the PID. A medium (order of 1–2 mm) precision two-dimensional detector can solve this task but the small available thickness (< 5 cm), the large final VHMPID size and the fact that the material budget had to be kept low which motivated us to choose the recently developed close cathode (CCC) chambers [27] with both strip and wire readout.

The CCC is a MWPC with specially built and powered wire plane that makes it insensitive to variations of the cathode–anode distance even if this distance is rather small (order of mm). The CCC has two advantages that are relevant for our application. One is that the tolerance to cathode–anode gap variations makes it unnecessary to build robust frames for the chamber thus minimizing the material and thickness. The other advantage is that the small gap limits the pad-response to practically one strip and the chamber can be read out digitally keeping the necessary spatial resolution.

For the beam test a small scale (64×64 mm^2 active surface, enough to cover the test-beam cross-section) with 2 mm pad-width and anode wire spacing has been built [28]. Both the front and rear units contain two CCC chambers to guarantee the reliable operation of the beam definition part of the test. One of the CCC chambers is shown in Fig. 19. The assembled chamber unit is shown in Fig. 20. The chambers are operated with Ar-CO2 80–20% mixture, the typical gas flow is few l/h.

3. Beam-test setup

The elements described in Section 2 were installed at the T-10 experimental zone located in the East Hall of the CERN PS accelerator to form the VHMPID prototype to be tested.

The T10 zone can provide electrons and pions of both signs contaminated with few kaons, protons, muons. The available momentum range is 1 to < 7 GeV/c.

The schematic drawing of the test setup with the radiator gas part is shown in Fig. 21. (The abbreviations on the drawing are as follows: BPD: Beam Position detector; PD: Photon detector; RGR: Radiator gas supply rack; RV: Radiator vessel; S: Scintillator; ThC: Threshold Cherenkov counter; TrM: Transparency-meter.) The picture of the equipment installed inside the beam zone is shown in Fig. 22. A closer view on the insulated (and heated) radiator and photon detector can be seen in Fig. 23.

The beam trigger was provided by two pairs of scintillators defining the 1×1 cm^2 triggered area and a 20×20 cm^2 scintillator fully covering the beam. The 4 m long threshold Cherenkov counter used for particle identification is a standard equipment of the beam line [29]. By changing the air (or CO_2) pressure between < 0.1 and 3 bar (depending also on the momentum of the incoming particle) it can be tuned to give signal for electrons only or for all types of particles (except protons). The output signal is either included in the trigger conditions or recorded for event tagging. The position and angle of the incoming particle were defined by the two BPD units providing about 1 mm and 1mrad precision.

The C_4F_8O gas cylinder and the radiator gas supply (both heated and insulated), the transparency-meter and the O_2 & H_2O analyzer were installed in the T10 gas area outside the experimental zone at about 20 m distance from the Cherenkov unit. A closer view of the transparency-meter and the O_2 & H_2O analyzer can be seen in Fig. 8, the insulated radiator gas supply rack and the C_4F_8O cylinder are shown in Fig. 10. The radiator gas supply and return lines were also heated and insulated. The pressure and heat control rack was located
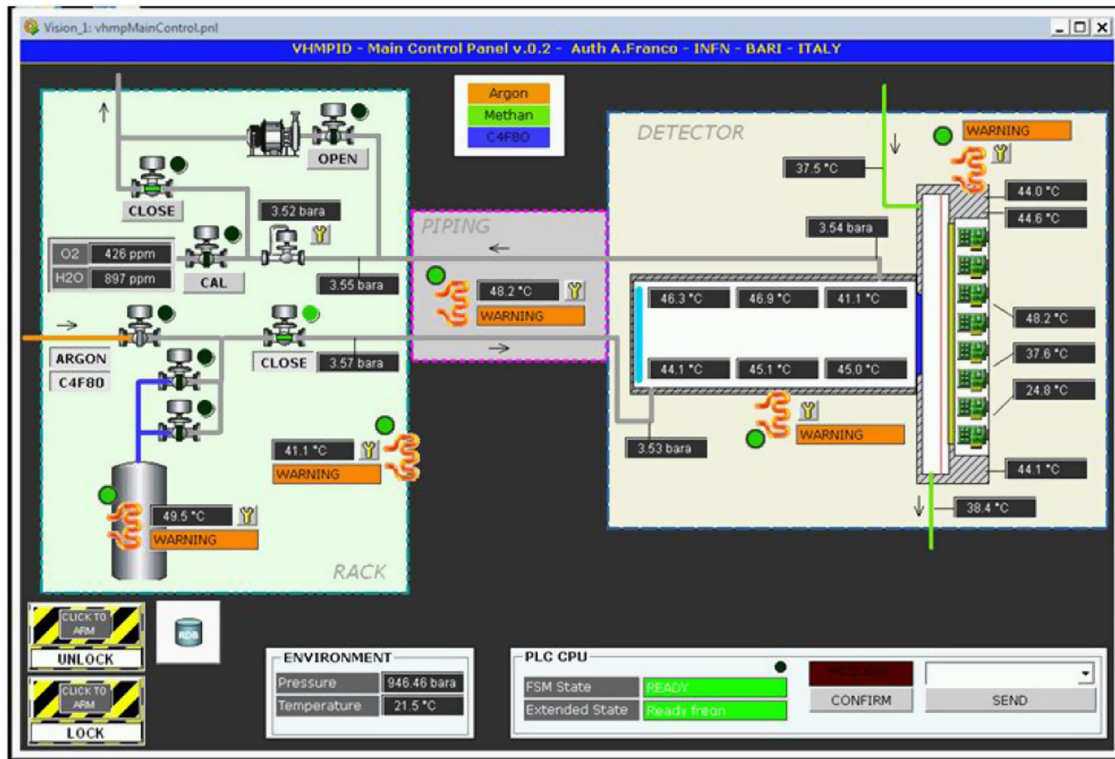
Fig. 17. The PVSS-panel of pressure and temperature control of the radiator gas.
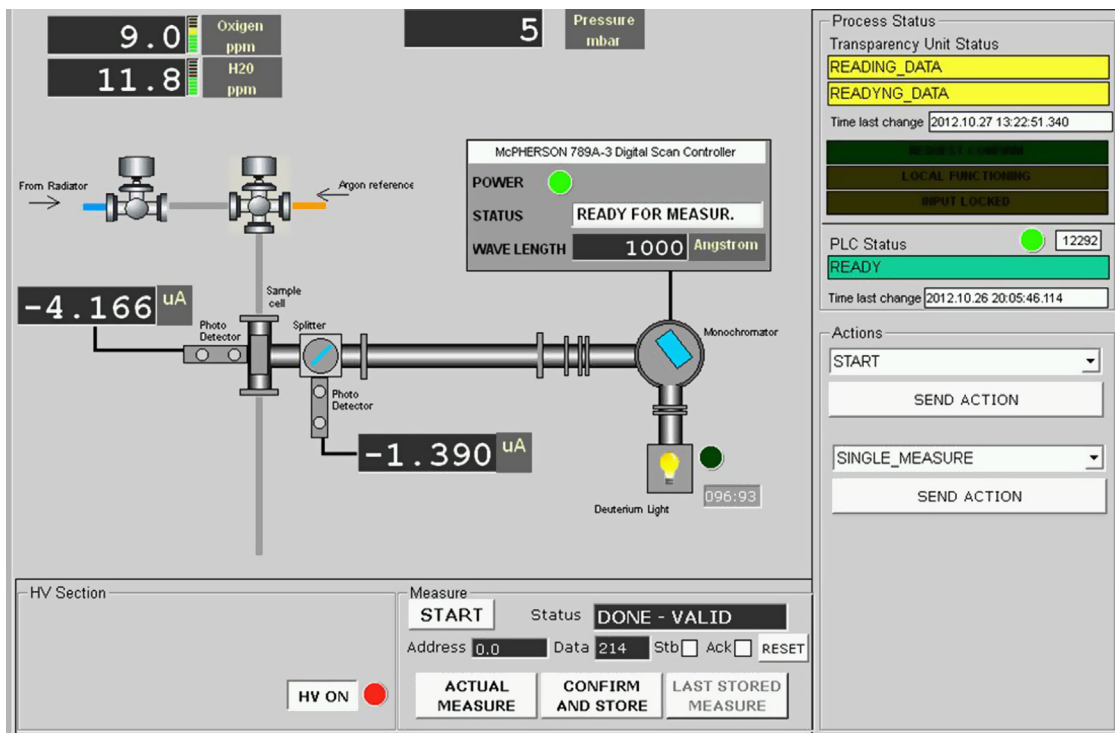

Fig. 18. The PVSS-panel of the transparency meter.

inside the zone close to the setup (see Fig. 22). CH_4, Ar and CO_2 were provided by the gas supply equipment belonging to the East hall and the T10 experimental zone.

The DAQ system was inherited from HMPID and matched well with the frontend.

4. Measurements and results

The beam test of the VHMPID prototype was carried out in October–November 2012 at the T10 experimental zone in the East Hall of the CERN PS accelerator.
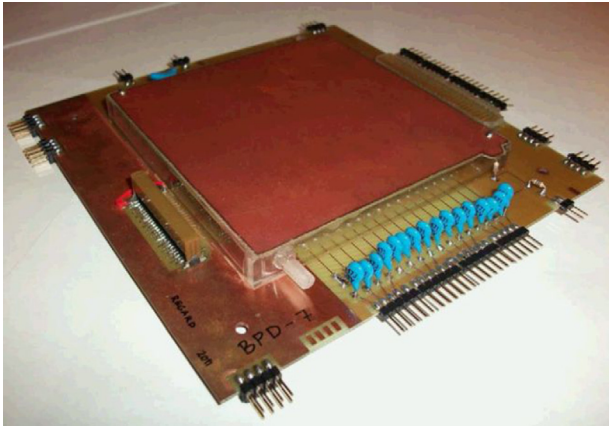
Fig. 19. The small scale (64×64 mm^2) CCC-prototype used to build the BPD detector.
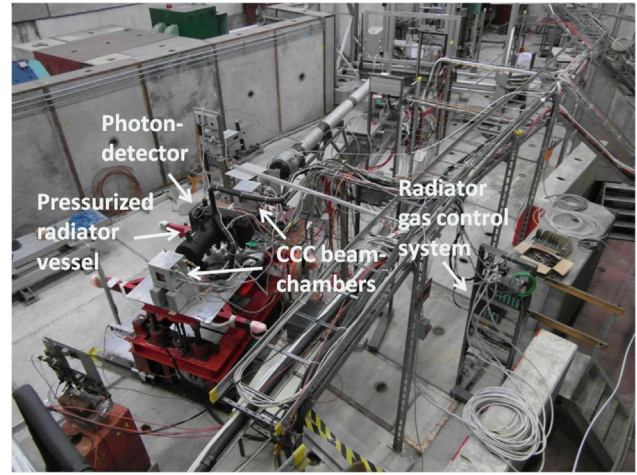
Fig. 22. The test prototype in the PS/T10 zone.
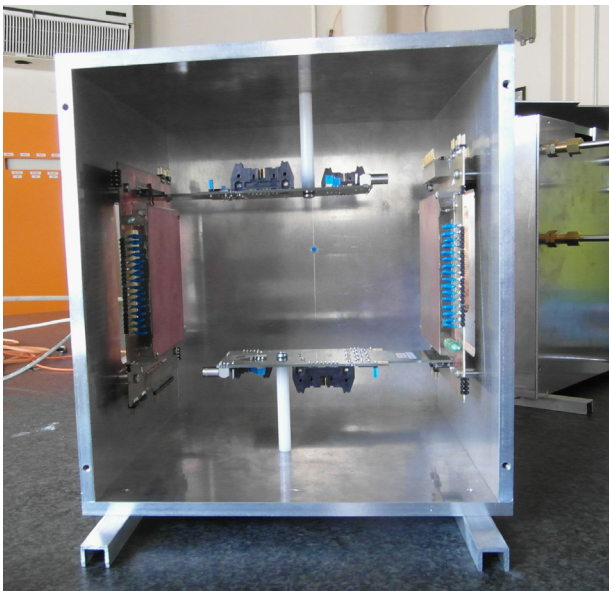
Fig. 20. The assembled BPD (Beam Positioning Detector).
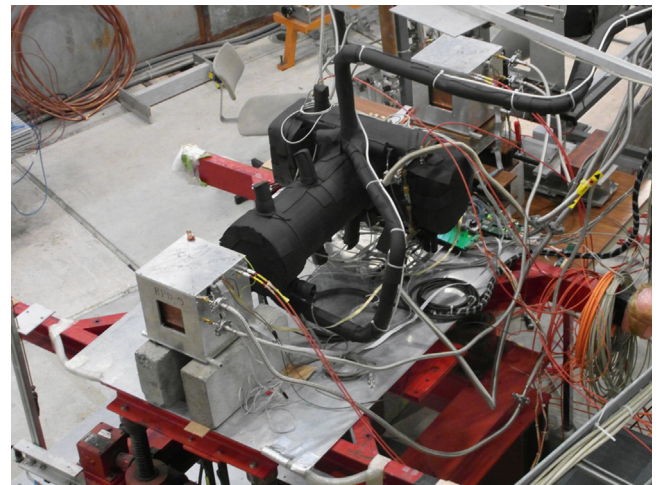

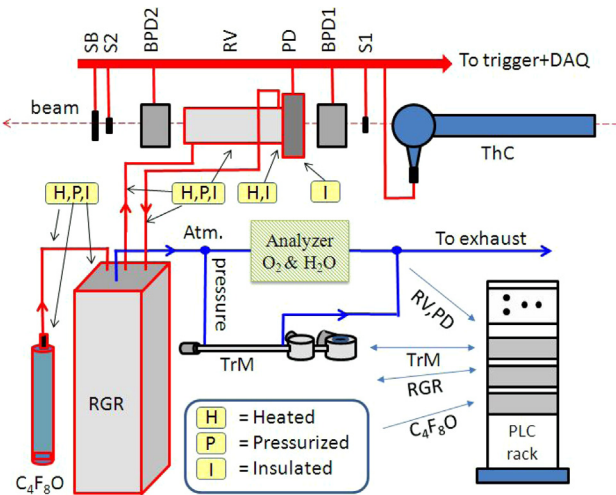**Fig. 23.** The radiator and photon detector part of the setup.

Fig. 21. The schematic drawing of the test setup (for the abbreviations see the text).

Data were taken at different beam and trigger conditions, varying parameters of the radiator gas (pressure, purity) and the photon detector (cathode–anode gap, high voltage). Due to the limited rate capability of the readout part (see section 2.2) the beam rate was kept low (< 20 kHz).

To achieve the best possible radiator gas quality, first the radiator gas system was filled and purged by several cycles of filling – heating vacuum-pumping with Ar. After applying this procedure the vessel was filled with radiator gas at atmospheric pressure, then heated and finally the pressure was gradually increased up to the nominal 3.5 bar (2.5 bar overpressure) level. The transparency and the O_2 & H_2O contamination levels were permanently measured and recorded. The spectral distribution of the radiator gas transparency and its variation are demonstrated in Fig. 24 where three measurements during the same day are shown. The degraded transparency (morning curve) was caused most probably by the outgassing of the reinforcing structure of the mirror and the inner wall of the vessel. Both could be compensated by the increase of the radiator gas flow and the radiator gas quality could be improved (evening curves).

As the aim of this paper is to describe the technical aspects of the VHMPID prototype and the beam-test setup the most characteristic results are presented here mainly to show the operation and performance of the prototype. More results (including those shown also here) and more studies are described in [1] and [2].

The analysis of the raw data, the determination of the ring fiducial zone, the cluster classification and deconvolution followed the procedure developed by the HMPID collaboration and
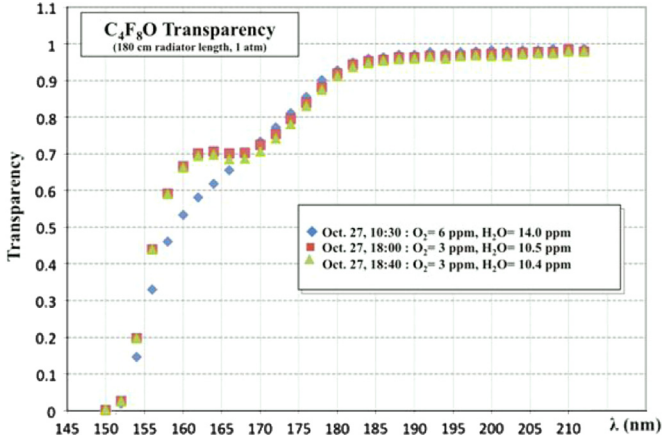
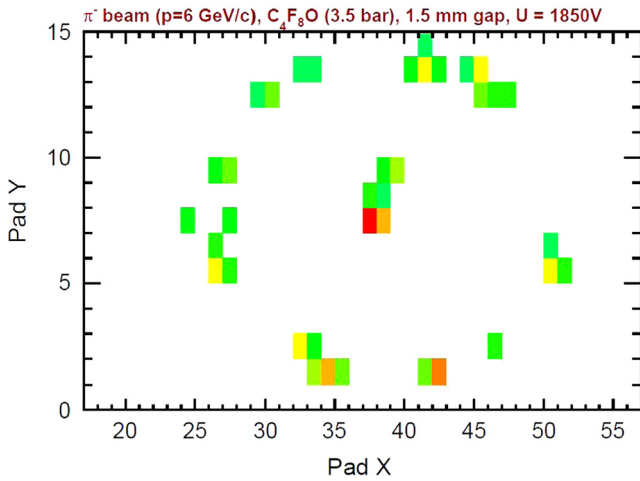**Fig. 24.** Three transparency measurements of the radiator gas during the same day.

Fig. 26. The Cherenkov angle distribution and the kaon–pion separation at 6 GeV/c beam momentum.

Fig. 25. A typical single event.

Fig. 27. The distribution of the photoelectron clusters in the Cherenkov-ring fiducial.

Fig. 28. The Cherenkov angle distribution for all pions with a momentum $p=6$ GeV/c.

described e.g. in section 3 of [30]. The results are summarized in Figs. 25, 26, 27, 28 and 29. A typical Cherenkov ring single event around the incoming particle is shown in Fig. 25. Fig. 26 shows the example of kaon–pion separation and the ring-radius distribution for 6 GeV/c pion beam containing small kaon contamination. The distribution of the detected photoelectron clusters in the Cherenkov-ring fiducial is shown in Fig. 27. The Cherenkov angle distribution for all pions with a momentum $p=6$ GeV/c with Gaussian fit is shown in Fig. 28.

The parameters of all the elements of the setup and the radiator gas transparency achieved during the test were introduced in a simulation describing the expected performance of the prototype. The simulation of the photon detector response to single photoelectrons emerging from the CsI photocathode was already performed for the HMPID detector study [30] and has been included in the present simulation. In Fig. 29 the measured testbeam results and the simulated values are compared for the Cherenkov angle for the particles tested.

Extrapolating the measured and simulated data (see Fig. 29) a good kaon–pion separation can be expected (at least) up to ~15 GeV/c. The upper part (15 to 25 GeV/c) of the momentum range is reachable at reduced pressure of the radiator gas. In this case the limiting factor might be the degrading PID efficiency due to the reduced number of generated photons and the smaller ring radius.
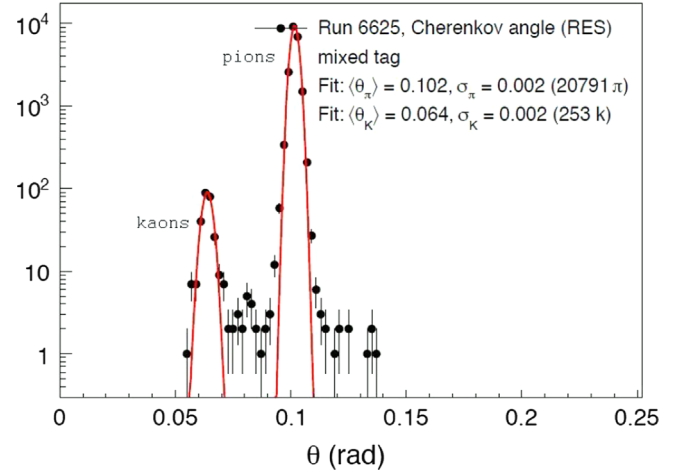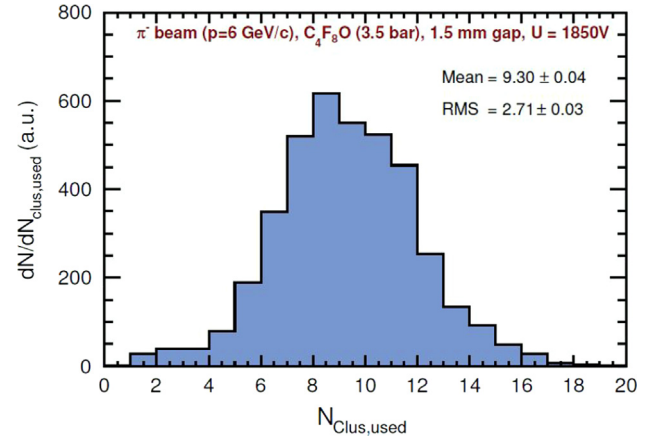
5. Conclusions

A test prototype of the VHMPID RICH detector proposed for the ALICE experiment at the CERN LHC accelerator has been designed, built and tested in particle beam at the CERN PS accelerator. The test results were compared with simulations. The good agreement indicates that the factors and processes determining the performance of the detector are known and well
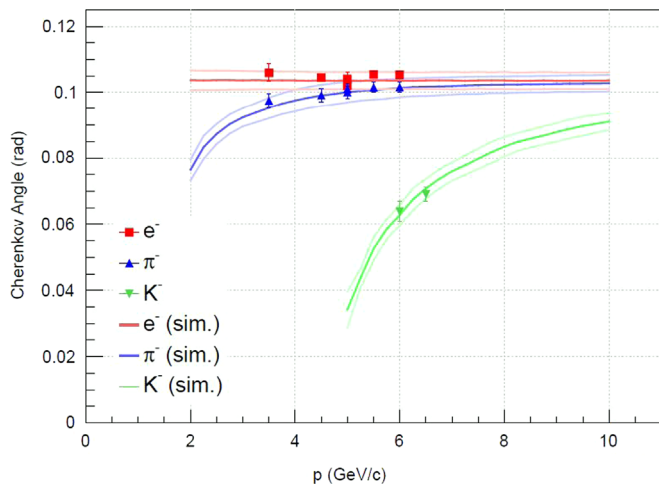
Fig. 29. Measured testbeam results and the simulated values are compared for the Cherenkov angle for the particles tested.

understood. In particular, the C_4F_8O radiator gas parameters in the VUV spectral range are very similar to those of C_4F_{10} so it is a suitable alternative to be used together with CsI based photon detectors. The results obtained during the test as the number of detected clusters or the Cherenkov ring radius resolution are fulfilling the requirements necessary to build a detector with the targeted PID capability.

Acknowledgments

References

[1] T.V. Acconcia, et al., The European Physical Journal – Plus 129 (2014) 91. http://dx.doi.org/10.1140/epjp/i2014-14091-5.
[2] A.G. Agocs, et al., Nuclear Instruments and Methods in Physics Research Section A 732 (2013) 361.
[3] G. Volpe, et al., Nuclear Instruments and Methods in Physics Research Section A 595 (2008) 40.
[4] A. Agocs, et al., Nuclear Instruments and Methods in Physics Research Section A 617 (2010) 424.
[5] A. Di Mauro, et al., Nuclear Instruments and Methods in Physics Research Section A 639 (2011) 274.
[6] B. Alessandro, et al., ALICE Collaboration, Journal of Physics G—Nuclear and Particle Physics 32 (2006) 1295.
[7] Technical Design Report of the ALICE HMPID Detector, CERN/LHCC 98-19, ALICE TDR 1, 14 August 1998.
[8] F. Piuz, et al., Nuclear Instruments and Methods in Physics Research Section A 433 (1999) 178.
[9] A. Braem, et al., Nuclear Instruments and Methods in Physics Research Section A 502 (2003) 205.
[10] A. Di Mauro, et al., Nuclear Instruments and Methods in Physics Research Section A 525 (2004) 173.
[11] J.-C. Santiard, Nuclear Instruments and Methods in Physics Research Section A 518 (2004) 498.
[12] G. Lenzen, et al., Nuclear Instruments and Methods in Physics Research Section A 343 (1994) 268.
[13] D. Ryckbosch, Nuclear Instruments and Methods in Physics Research Section A 433 (1999) 98.
[14] S. Korpar, et al., Nuclear Instruments and Methods in Physics Research Section A 433 (1999) 128.
[15] K. Zeitelhack, et al., Nuclear Instruments and Methods in Physics Research Section A 433 (1999) 201.
[16] P. Abbon, et al., Nuclear Instruments and Methods in Physics Research Section A 577 (2007) 455.
[17] S. Horikawa, et al., Nuclear Instruments and Methods in Physics Research Section A 595 (2008) 212.
[18] M. Adinol, et al., The European Physical Journal C 73 (2013) 2431.
[19] M. Salvi-Narkhede, et al., The Journal of Chemical Thermodynamics 25 (1993) 643.
[20] Tomasz Skwarnicki, Nuclear Instruments and Methods in Physics Research Section A 553 (2005) 339.
[21] M. Artuso, et al., Nuclear Instruments and Methods in Physics Research Section A 558 (2006) 373.
[22] E. Albrecht, et al., Nuclear Instruments and Methods in Physics Research Section A 502 (2003) 266.
[23] A. Di Mauro, et al., 4th IEEE International Workshop on Advances in Sensors and Interfaces (IWASI), 2011, p. 203.
[24] P.-S. Silva, CERN Safety Requirements for Pressure Equipment.
[25] See link e.g. in 〈http://www.netmarkscom.com/crystalsystems/sapph_optical_properties.html〈 from Crystal Systems Inc. (MA, USA).
[26] G.J. Barber, et al., Nuclear Instruments and Methods in Physics Research Section A 593 (2008) 624.
[27] D. Varga, et al., Nuclear Instruments and Methods in Physics Research Section A 648 (2011) 163.
[28] D. Varga, et al., Nuclear Instruments and Methods in Physics Research Section A 698 (2013) 11.
[29] M. Vivargent, et al., Nuclear Instruments and Methods 22 (1963) 165.
[30] A. Di Mauro, et al., Nucl. Instr. and Methods A 433 (1999) 190.